

Determination of the polarizability of Na-like silicon by study of the fine structure of high- L Rydberg states of Si^{2+}

R. A. Komara, M. A. Gearba, and S. R. Lundeen

Department of Physics, Colorado State University, Fort Collins, Colorado 80523, USA

C. W. Fehrenbach

Department of Physics, Kansas State University, Manhattan, Kansas 66502, USA

(Received 2 March 2003; published 13 June 2003)

The fine-structure intervals in the $n=29$ state of Si^{2+} separating levels from $L=8$ to $L=14$ have been measured by microwave spectroscopy. A beam of Si^{3+} (Na-like silicon) captures a single electron from an $n=10$ Rydberg target, forming highly excited Rydberg states of Si^{2+} near $n=29$. Specific L levels within $n=29$ are selectively detected by excitation with a Doppler-tuned CO_2 laser, followed by Stark ionization. This allows the detection of microwave induced transitions between different L levels in the $n=29$ state, determining the fine-structure intervals. The fine-structure pattern can be used to deduce the dipole polarizability of the Si^{3+} ion, which forms the core of the Rydberg system. The result $\alpha_d=7.404(11)$ is in good agreement with calculations that are comparable in precision.

DOI: 10.1103/PhysRevA.67.062502

PACS number(s): 32.10.Dk, 32.10.Fn, 32.30.Bv

I. INTRODUCTION

The fine structure of nonpenetrating high- L Rydberg states can be attributed to a long-range interaction potential with the positive-ion core, the leading term of which, for s -state cores, is the dipole polarization energy [1,2]. Because of this, measurements of high- L Rydberg fine structure can be used to deduce precise values of core polarizabilities [3]. The Rydberg electron acts as a sensitive probe of this property of the ion core. Precise measurements of atomic and ionic polarizabilities provide a challenging test of atomic structure calculations. This is particularly valuable in the case of alkali-metal atoms and alkali-metal-like ions, since the theory has been highly developed in those cases in order to support tests of atomic parity violation and searches for electron electric dipole moments. A number of new experimental techniques have been developed in order to make precise measurements of polarizabilities of neutral alkali-metal atoms [4,5]. Measurements with these techniques are approaching the level of precision of 0.1%. Measurements of singly charged ion polarizabilities by Rydberg spectroscopy have already achieved this level of precision. Examples are the 0.005% measurement of the polarizability of H_2^+ and D_2^+ [3], the 0.10% measurement of the polarizability of Ne^+ [1], and precise measurements of the polarizability of Cs^+ [6]. Many of these measurements were made using the resonant excitation Stark ionization spectroscopy (RESIS) method in which Rydberg states are formed in a fast beam, selectively detected with laser excitation, and studied carefully with microwave spectroscopy. Until now, however, this technique has been limited to neutral Rydberg states, and therefore to studying singly charged ions. Recently, however, the selective detection of high- L Rydberg states of multiply charged ions has been demonstrated with this technique [7]. The key to this advance was using a selectively excited Rydberg target to form the Rydberg ions by single-electron charge transfer. This populates a narrow range of highly excited states at

about the right binding energy to be efficiently detected with a CO_2 laser. We report here the use of microwave spectroscopy on these Rydberg ions, obtaining a map of the $n=29$ Rydberg levels of Si^{2+} with $8 \leq L \leq 14$. Fitting the fine structure of these levels to the long-range interaction model yields a precise value of the dipole polarizability of the Na-like Si^{3+} ion which is at the core of this Rydberg system.

II. EXPERIMENT

Figure 1 illustrates the apparatus used for this measurement. A 12-keV beam of Si^{3+} ions is obtained from the 5-GHz electron cyclotron resonance (ECR) ion source at the J.R. Macdonald Laboratory at Kansas State University. The ions are passed through a dense $n=10$ Rydberg target [8] where a few percent of them capture a single electron, populating levels near $n=29$ in Si^{2+} . Immediately after charge capture, all the ions enter the “repeller” region, a double einzellens with potentials chosen to block the remaining Si^{3+} ions while transmitting and refocusing the Si^{2+} ions. Ions remaining in a particular L level within $n=29$ are detected

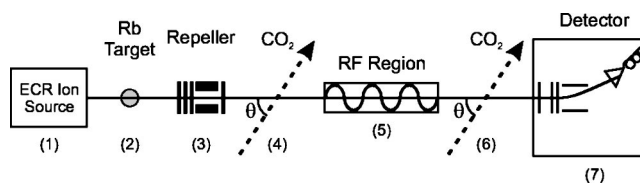


FIG. 1. Diagram of components used in the RESIS technique. A Si^{3+} beam is extracted from the ECR source at (1). Some of the ions capture an electron from the $10F$ Rb target (2). The remaining primary ion beam is reflected and upper Rydberg states in the Si^{2+} beam are field ionized in the repeller (3). A Doppler-tuned CO_2 laser drives specific $(n,L)-(n',L')$ transitions within the remaining charge transfer beam at (4) and (6). Microwave transitions between L states are induced in the transmission line microwave region at (5). Signal ions are then Stark ionized and deflected into a channeltron for detection (7).

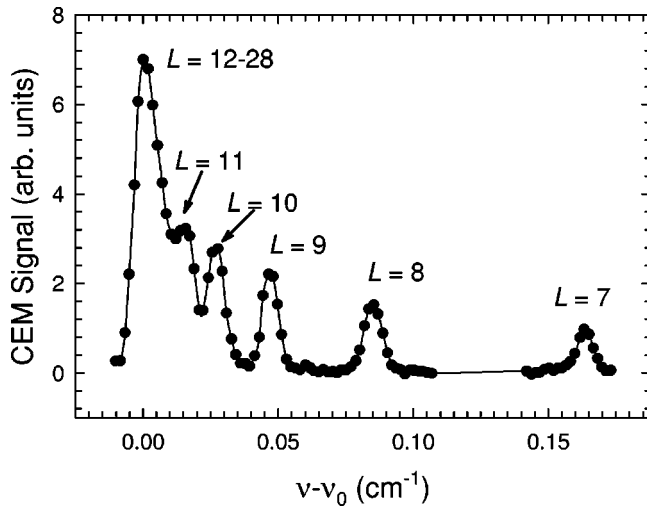


FIG. 2. Measured ion current resulting from excitation of the $n=29$ to 90 transition in Si^{2+} vs the difference between the Doppler-tuned CO_2 laser frequency and the hydrogenic transition energy. Levels within $n=29$ with L from 7 to 11 are resolved. The unresolved $L > 11$ levels form the large peak near the hydrogenic transition energy.

by exciting them to the $n=90$ level using a Doppler-tuned CO_2 laser [at (6) in Fig. 1] and then Stark ionizing the $n=90$ level and collecting the resulting Si^{3+} ion [at (7) in Fig. 1]. The arrangement of ionizing electrodes within the Rydberg detector is such that the ionization of $n=90$ takes place at a negative potential, resulting in an energy difference between the Si^{3+} ions that result from laser excitation and any others that may be present as a result of collisional ionization. Figure 2 shows an example of the ionization current observed as a function of the Doppler-tuned CO_2 laser frequency. The laser resolution, limited by the angular spread of the ion beam, is sufficient to fully resolve individual fine-structure levels within $n=29$ with L up to 11 .

Before they reach the detection region described above, the ions pass through a microwave interaction region where they are subjected to a microwave electric field which may induce transitions between two fine-structure levels. If a population difference exists between these two levels, these transitions will change the population of both levels and result in a change in the ionization current measured in the detector when the CO_2 laser is tuned to excite either of the levels. This population change can be measured as a function of the microwave frequency to display the transition resonance. An example is shown in Fig. 3 which illustrates the transition between $L=9$ and $L=10$ levels within $n=29$. In order to enhance the size of such signals, a second CO_2 interaction region is used at (4) in Fig. 1 to deplete one of the two levels by exciting it to the $n=90$ level using the same transition later used to detect the remaining population. For example, the resonance of Fig. 3 was obtained with both CO_2 laser interactions tuned to excite the $(n,L)=(29,9)$ to $(90,10)$ transition.

For this study, similar transition resonances were observed for transitions for $L-L'$ of $8-9$, $9-10$, $10-11$, and $11-12$. In addition, two- and three-photon transitions were ob-

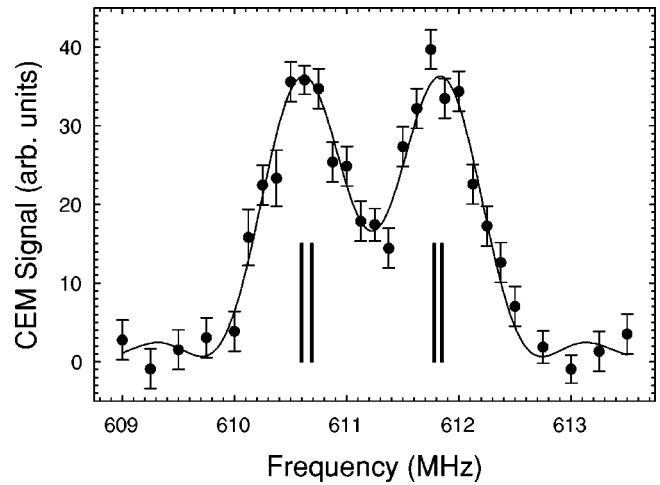


FIG. 3. Resonance line shape for the $(n,L)=(29,9)$ to $(29,10)$ transition in Si^{2+} measured with the microwaves traveling antiparallel to the Si^{2+} beam. The vertical bars represent the calculated spin structure and the solid line is the best fit to the theoretical line shape.

served from $11-13$ and $11-14$, respectively. As illustrated in Fig. 3, the frequency resolution of the microwave resonances was about 1 MHz, sufficient to partially resolve structure due to the two-electron spins. This is dominated by the spin-orbit interaction for the Rydberg electron, with a smaller contribution from the spin of the core electron. The latter is modified by an indirect spin-orbit interaction coming from virtual excitation of the core [9]. The calculated spin structure for the $9-10$ transition is shown by a stick diagram in Fig. 3. Since, within the resolution of the measurement, this is indistinguishable from the simple hydrogenic spin-orbit interaction, the resonance lines were fit to a superposition of two lines of equal amplitude split by this calculated spin splitting. A small correction was applied to the fitted centers so that the quoted transition energy corresponds to the energy difference between the centers of gravity of the two hydrogenic spin levels. Since the two components were not well resolved in the case of the higher- L transitions, an additional error equal to 5% of the spin splitting was added to the statistical error from the fits to account for the uncertainty of the relative component strengths. For each interval, transitions were measured for both directions of propagation of the microwave traveling wave, parallel and antiparallel to the beam velocity. The geometric mean of the transition energy in the two cases gives the transition frequency for stationary ions. In the case of the two- and three-photon transitions, ac Stark shift corrections were calculated and applied to the results. The measured fine-structure intervals are shown in Table I, column 2.

The major experimental difficulty in this work was the control of stray electric fields that were observed to build up within the microwave interaction region by charging of nominally conducting surfaces. The presence of these fields was confirmed by observations, using the same interaction region, of the 10 G-H transition in helium, whose true position and Stark shift rate are well known from previous measurements [10]. These studies indicated that stray fields in

TABLE I. Measured values of $n=29$ fine-structure intervals. Column 1 gives L and L' for the observed interval. Column 2 gives the measured interval, in the presence of the ambient stray electric field. Column 3 shows the Stark shift rate κ for the interval in $\text{MHz}/(\text{V}/\text{cm})^2$, and column 4 shows the inferred value of the interval in the absence of electric fields. The fitted value of the stray field is $0.110(10)$ V/cm. The second-order energy corrections are listed in column 5.

Interval	ΔE_{obs} (MHz)	κ	$\Delta E_{E=0}$ (MHz)	$\Delta E^{[2]}$ (MHz)
8–9	1160.703(35)	–13.7	1160.87(5)	2.422
9–10	611.461(48)	–25.2	611.77(7)	0.657
10–11	343.491(70)	–34.7	343.91(10)	0.202
11–12	203.143(52)	–49.8	203.75(15)	0.070
11–13	328.24(11)	–111.9	329.60(27)	0.095
11–14	408.20(19)	–191.1	410.51(46)	0.106
12–13	125.10(12)	–62.1	125.85(18)	0.025
13–14	79.96(22)	–79.2	80.91(28)	0.011

the range of 100–200 mV/cm could be present within the interaction region, and also that the size of the field changed over time, especially during the process of changing between Si^{3+} and He^+ beams. On the other hand, the stray field was nearly constant over long periods of time when only the Si^{3+} ion beam was used. Because the stray field was constant under these circumstances, its size could be determined from the pattern of fine-structure intervals measured in Si^{2+} , which is significantly altered by the Stark shifts. By including the ambient electric field as a fitting parameter in analyzing the observed fine-structure intervals, as described below, it was possible to learn the size of the field present during the data collection and to correct the observed intervals for its effect.

III. ANALYSIS

The long-range potential model predicts that the binding energy of high- L Rydberg levels is given by

$$E(n, L) = E^{[0]}(n) + E_{rel}(n, L) - \frac{\alpha_d}{2} \langle r^{-4} \rangle_{n, L} - \left(\frac{\alpha_Q}{2} - 3\beta_d \right) \times \langle r^{-6} \rangle_{n, L} - C_8 \langle r^{-8} \rangle_{n, L} + E^{[2]} + \dots, \quad (1)$$

where $E^{[0]}(n)$ is the hydrogenic energy, α_d and α_Q are the adiabatic dipole and quadrupole polarizabilities of the core, β_d is the first nonadiabatic correction to the dipole polarizability, and C_8 accounts for higher-order terms. E_{rel} is the relativistic correction to the electron's kinetic energy,

$$E_{rel}(n, L) = - \frac{\alpha^2 Z^4}{2n^3(L + \frac{1}{2})} \text{ a.u.}, \quad (2)$$

where Z is the core charge, and $E^{[2]}$ is small correction due to the second-order effects of the leading dipole polarization potential [11]. The radial expectation values are assumed to take their hydrogenic values [12], accounting for both the charge and mass of the core ion. In the absence of Stark shifts, the fine-structure intervals are given by

$$\Delta E = \Delta E_{rel} + \Delta E^{[2]} + \frac{\alpha_d}{2} \Delta \langle r^{-4} \rangle + \left(\frac{\alpha_Q}{2} - 3\beta_d \right) \Delta \langle r^{-6} \rangle + C_8 \Delta \langle r^{-8} \rangle + \dots \quad (3)$$

The Stark shift rate of each fine-structure interval can be calculated from hydrogenic matrix elements and the measured fine-structure intervals, assuming that all m states are equally populated. The relative shift rates among the several transitions are only weakly dependent on these assumptions. Column 2 of Table I shows these calculated rates for the six transitions studied. Since measurements showed that the stray field was not entirely constant during data collection, an additional uncertainty equal to 5% of the Stark shift was added to each measured transition energy.

In order to extract a value of α_d from the measured intervals, and illustrate the data pattern conveniently, the measured intervals were corrected for the calculated relativistic contributions and second-order polarization effects and then divided by the calculated $\Delta \langle r^{-4} \rangle$ values. The resulting quantities, all of the same order of magnitude, were then fit to a function of the form

$$\frac{\Delta E_{obs} - \Delta E_{rel} - \Delta E^{[2]}}{\Delta \langle r^{-4} \rangle} = A_4 + A_6 \frac{\Delta \langle r^{-6} \rangle}{\Delta \langle r^{-4} \rangle} + A_8 \frac{\Delta \langle r^{-8} \rangle}{\Delta \langle r^{-4} \rangle} + A_E \frac{\kappa}{\Delta \langle r^{-4} \rangle}, \quad (4)$$

where the coefficients A_i represent the coefficients in Eq. (3) and κ is the Stark shift rate from Table I. All terms are expressed in atomic units. The results of this fit are illustrated in Fig. 4 by the dashed line connecting triangles. The fitted coefficient A_E gives our best estimate of the stray field present within the microwave interaction region at the time of data collection. It gives a result well within the range of fields indicated by the helium diagnostic. Knowing the value of the stray field, the measured intervals can be corrected to indicate the intervals that would be measured at zero field. These are shown in Table I, column 4, and also illustrated in Fig. 4 by the solid circles. The smooth solid curve in Fig. 4

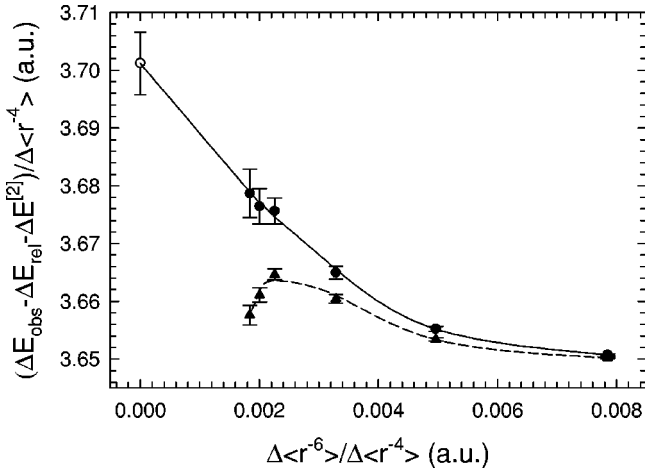


FIG. 4. Measured fine-structure intervals within the $n=29$ level of Si^{2+} , scaled and plotted as described in the text. The triangles illustrate the directly observed intervals, which are slightly Stark shifted by an ambient stray electric field. The dashed curve illustrates the fit to these observations, using Eq. (4) of the text. The solid circles and solid curve illustrate the inferred intervals in the absence of stray electric fields. The zero intercept of the solid curve gives the dipole polarizability of Si^{3+} .

illustrates the function of Eq. (4) using the fitted values of A_4 , A_6 , and A_8 . The intercept of this curve gives our best estimate of the polarizability α_d of the core ion,

$$(\alpha_d)_{\text{experiment}} = 2A_4 = 7.404(11)a_0^3. \quad (5)$$

The other fit parameters are $A_6 = -14.5(1.6)$, $A_8 = 843(115)$, and $A_E = 0.0121(22)$. The measured polarizability is in good agreement with a recent calculation [13,14],

$$(\alpha_d)_{\text{theory}} = 7.418(10)a_0^3.$$

The dominant contribution comes from the $3s\text{-}np$ mixing, which in turn depends directly on the calculated electric di-

pole matrix elements. The same matrix elements also predict the lifetimes of excited p states, but these are much harder to measure with high precision. The good agreement between measured and calculated polarizabilities adds to the confidence in calculations by similar methods which have been used to interpret experimental measurements of parity non-conserving matrix elements in atomic Cs [15]. It would be even more valuable to have such checks for heavier ions where relativistic effects are more dominant.

In summary, this paper demonstrates that experimental methods very similar to those used in the past to measure the polarizabilities of singly charged positive ions through the study of neutral high- L Rydberg states can also be used successfully to determine the polarizabilities of multiply charged ions. It remains to be seen what range of ion charges can be effectively studied with these methods. To date, Rydberg ions with charge up to 10 have been detected with the RESIS method [7]. There is no fundamental obstacle to the study of ions of arbitrary charge, but the experiments become steadily more difficult as the ion charge increases, largely because the principal quantum number of the levels accessed increases like the charge, giving each specific (n, L) level a smaller fraction of the total population. In principle, the method should be equally applicable to s -state and non- s -state ions, although the former will be much easier to study because of their simpler fine structure. The combination of wide applicability and high precision should make this technique a valuable addition to the list of experimental methods, which can be used to measure atomic polarizabilities.

ACKNOWLEDGMENTS

The authors thank Richard Drachman, Andrei Derevianko, Marianna Safronova, and Sergey Porsev for their helpful discussions. This work was supported by the Chemical Sciences, Geosciences, and Biosciences Division of the Office of Basic Energy Sciences, Office of Science, U.S. Department of Energy.

-
- [1] R.F. Ward, Jr., W.G. Sturuss, and S.R. Lundeen, *Phys. Rev. A* **53**, 113 (1996).
 - [2] W. Clark, C.H. Greene, and G. Miecznik, *Phys. Rev. A* **53**, 2248 (1996).
 - [3] P.L. Jacobson, D.S. Fisher, C.W. Fehrenbach, W.G. Sturuss, and S.R. Lundeen, *Phys. Rev. A* **56**, R4361 (1997).
 - [4] C.R. Ekstrom, J. Schmiedmayer, M.S. Chapman, T.D. Hammond, and D.E. Pritchard, *Phys. Rev. A* **51**, 3883 (1995).
 - [5] J. Amini and H. Gould, *Bull. Am. Phys. Soc.* **47** (3), 25 (2002).
 - [6] K.H. Weber and C.J. Sansonetti, *Phys. Rev. A* **35**, 4650 (1987).
 - [7] D.S. Fisher, S.R. Lundeen, C.W. Fehrenbach, and B.D. DePaola, *Phys. Rev. A* **63**, 052712 (2001).
 - [8] C.W. Fehrenbach, S.R. Lundeen, and O.L. Weaver, *Phys. Rev. A* **51**, R910 (1995).
 - [9] E. L. Snow (private communication).
 - [10] G.D. Stevens and S.R. Lundeen, *Phys. Rev. A* **60**, 4379 (1999).
 - [11] G.W.F. Drake and R.A. Swainson, *Phys. Rev. A* **44**, 5448 (1991).
 - [12] K. Bockasten, *Phys. Rev. A* **9**, 1087 (1973).
 - [13] M. S. Safronova (private communication).
 - [14] M.S. Safronova, W.R. Johnson, and A. Derevianko, *Phys. Rev. A* **60**, 4476 (1999).
 - [15] C.S. Wood *et al.*, *Science* **275**, 1759 (1997).